Pathogens and Disease, 76, 2018, fty043

doi: 10.1093/femspd/fty043
Advance Access Publication Date: 23 April 2018
Research Article

RESEARCH ARTICLE

Hypoxia arising from concerted oxygen consumption by neutrophils and microorganisms in biofilms

Yilin Wu[1], Isaac Klapper[1] and Philip S. Stewart[2,*]

[1]Department of Mathematics, Temple University, Philadelphia, PA 19122, USA and [2]Center for Biofilm Engineering and Department of Chemical and Biological Engineering, Montana State University, Bozeman, MT 59717-3980, USA

*Corresponding author: Center for Biofilm Engineering, 366 Barnard Hall, Montana State University, Bozeman, MT 59717-3980. Tel: +406 994 1960; Fax: +406 994 6098; E-mail: phil_s@montana.edu

One sentence summary: Biofilms and white blood cells that surround them during infection both contribute to localized depletion of oxygen.

Editor: Thomas Bjarnsholt

ABSTRACT

Infections associated with microbial biofilms are often found to involve hypoxic or anoxic conditions within the biofilm or its vicinity. To shed light on the phenomenon of local oxygen depletion, mathematical reaction-diffusion models were derived that integrated the two principal oxygen sinks, microbial respiration and neutrophil consumption. Three simple one-dimensional problems were analyzed approximating biofilm near an air interface as in a dermal wound or mucus layer, biofilm on an implanted medical device, or biofilm aggregates dispersed in mucus or tissue. In all three geometries considered, hypoxia at the biofilm–neutrophil interface or within the biofilm was predicted for a subset of plausible parameter values. The finding that oxygen concentration at the biofilm–neutrophil juncture can be diminished to hypoxic levels is biologically relevant because oxygen depletion will reduce neutrophil killing ability. The finding that hypoxia can readily establish in the interior of the biofilm is biologically relevant because this change will alter microbial metabolism and persistence.

Keywords: infection; biomaterial; medical device; innate immune

Nomenclature

C_A: oxygen concentration on biofilm-air boundary
C_B: oxygen concentration in biofilm region
C_H: oxygen concentration on biofilm-host boundary
C_N: oxygen concentration in neutrophil region
D_B: effective diffusion coefficient of oxygen in biofilm region
D_N: effective diffusion coefficient of oxygen in neutrophil region
h_B: slab thickness of biofilm region
h_N: slab thickness of neutrophil region
k_B: first-order oxygen reaction rate coefficient in biofilm region
k_N: first-order oxygen reaction rate coefficient in neutrophil region
r: spatial coordinate in spherical coordinates
R: combined radius of biofilm and neutrophil regions
r_B: radius of biofilm region
r_N: dimension of radial shell describing neutrophil region
z: spatial coordinate in slab geometry
$\emptyset_B$: biofilm region Thiele modulus
$\emptyset_N$: neutrophil region Thiele modulus

INTRODUCTION

A biofilm is a dense aggregation of microorganisms that are embedded in a hydrated polymer matrix of their own secretion (Hall-Stoodley, Costerton and Stoodley 2004). In the biofilm state, microbes evade killing by antibiotics and by the host

Received: 13 October 2017; **Accepted:** 20 April 2018

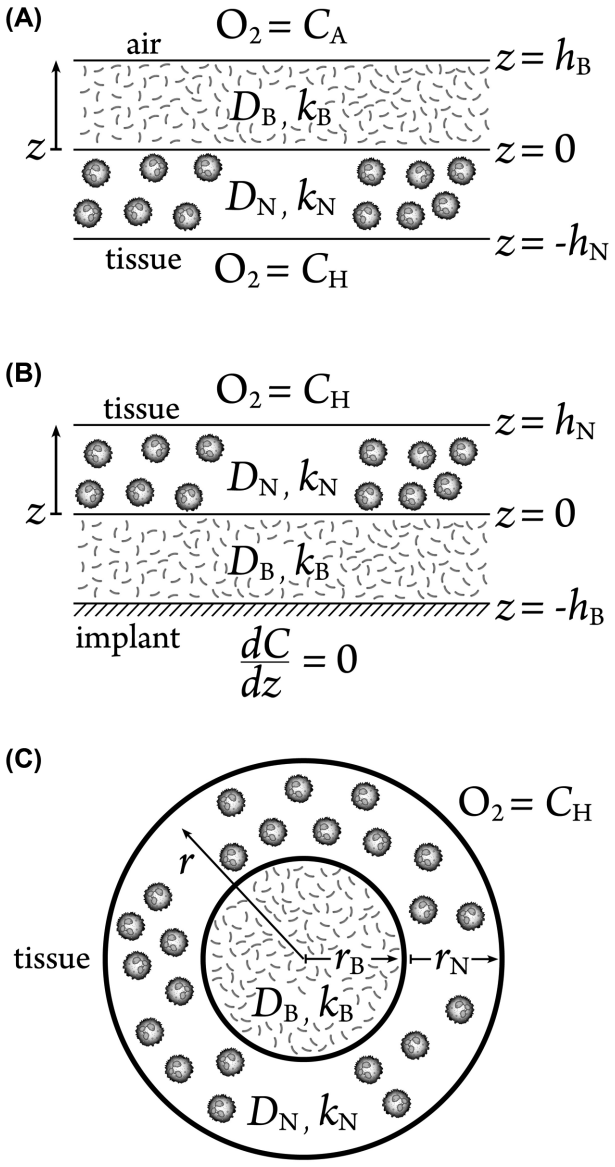

Figure 1. Assumed geometry of biofilm–neutrophil systems. (**A**) 1D two-layer slab geometry in which adjoining biofilm and neutrophil layers are bounded by oxygen sources on both external boundaries. One boundary is conceptualized as air and the other as host tissue. This geometry could approximate a biofilm in a dermal wound or in the airways of the lung. (**B**) 1D two-layer slab geometry in which a biofilm layer coats an impermeable surface and is covered by a second layer of neutrophils. This geometry could approximate the situation on an infected medical implant. (**C**) 1D spherical geometry in which a biofilm core is surrounded by a concentric spherical shell of neutrophils. This geometry could approximate a biofilm aggregate in mucus or deep tissue.

defenses (Costerton, Stewart and Greenberg 1999; Donlan and Costerton 2002). Examples of infections that are now widely acknowledged to stem from biofilms include periodontitis (gum disease) (Pihlstrom, Michalowicz and Johnson 2005); chronic lung infection in individuals with cystic fibrosis (CF) (Costerton, Stewart and Greenberg 1999; Lyczak, Cannon and Pier 2002); chronic wounds such as diabetic foot ulcers, pressure ulcers and venous stasis ulcers (Bjarnsholt *et al.* 2008; James *et al.* 2008); and troublesome infections associated with implanted medical devices such as catheters (Passerini *et al.* 1992; Morris, Stickler and McLean 1999), heart valves (Hyde, Darouiche and Costerton 1998) and artificial joints (Gristina *et al.* 1994). Biofilm formation is thus a common microbial strategy that is considered a virulence factor in numerous persistent infections (Costerton, Stewart and Greenberg 1999).

A nearly universal feature of microbial biofilms in oxic environments is an oxygen concentration gradient (Xu *et al.* 1998; Stewart 2003). Respiring microbes at the surface of the biofilm consume oxygen creating an oxygen shadow that alters microbial metabolism and allows for the coexistence of aerobic and anaerobic microorganisms in close proximity. Multiple lines of evidence indicate oxygen limitation and a shift to anaerobic metabolism in biofilm infections. Here we focus discussion on CF pneumonia and chronic wounds.

One of the most compelling pieces of evidence for hypoxia in infected non-healing wounds is the identification of strictly anaerobic bacteria, such as those belonging to the genera *Bacteroides* and *Clostridia*, which are commonly found in human chronic wounds (Dowd *et al.* 2008; Frank *et al.* 2009; Frankel *et al.* 2009; Price *et al.* 2009; Han *et al.* 2011). The presence of these microorganisms, which require highly reduced conditions to be able to multiply, shows that anoxic niches occur in these infected tissues. In addition, direct measurement of very low skin tissue oxygenation in the vicinity of chronic wounds has been reported and shown to correlate with impaired healing (Kalani *et al.* 1999; Ruangsetakit *et al.* 2010). Neutrophils are known to be abundant in chronic ulcers (Diegelmann 2003).

The lung is a well-aerated environment. In the CF lung, however, thickened mucus and deficient mucociliary clearance combine to permit overgrowth of bacteria and localized depletion of oxygen. Invading neutrophils, the predominant inflammatory cells (Downey, Bell and Elborn 2009) consume oxygen as do the bacteria (Kolpen *et al.* 2010). Anoxic pockets within the infected mucosa (Worlitzsch *et al.* 2002) or freshly expectorated infected sputum (Kolpen *et al.* 2014; Cowley *et al.* 2015) have been directly measured using oxygen microelectrodes. Recent investigations also report the recovery of large numbers of anaerobic bacteria from the airways of CF patients when appropriate techniques are employed (Tunney *et al.* 2008; Guss *et al.* 2011; Sibley *et al.* 2011; Zemanick, Sagel and Harris 2011). These chemical and biological measurements are consistent with hypoxic conditions within the lung mucus layer. Even the paradigm CF pneumonia organism *Pseudomonas aeruginosa*, widely understood to prefer aerobic growth conditions, is now thought to grow under microaerobic or anaerobic conditions *in vivo* in the CF lung (Costerton 2002; Yoon *et al.* 2002; Alvarez-Ortega and Harwood 2007; Hassett *et al.* 2009; Schobert and Jahn 2010; Kolpen *et al.* 2014). Oxygen limitation and a shift to anaerobic metabolism are hallmarks of biofilm infection (Stewart *et al.* 2016).

Oxygen concentration is a critical parameter for host healing (Sen and Roy 2008; Sen 2009), neutrophil function and signaling (Mandell 1974; Klebanoff 1980; Goldberg *et al.* 1995; Campbell *et al.* 2014; Taylor *et al.* 2016), and microbial persistence (Borriello *et al.* 2004; Field *et al.* 2005; King *et al.* 2010; Schaible, Taylor and Schaffer 2012; Gupta, Laskar and Kadouri 2016). We hypothesize that local oxygen concentration plays a fundamental role in the etiology of biofilm infection. Both host and microbe consume oxygen, modulate oxygen transport and actively respond to oxygen, giving rise to complex interactions with multiple feedback loops (Jensen *et al.* 1990; Jesaitis *et al.* 2003; Campbell *et al.* 2014; Taylor *et al.* 2016). The purpose of the work reported here is to provide a starting place for analyzing the concerted utilization of oxygen by microorganisms in a biofilm and neutrophils responding to the microbial aggregate. This work expands on many years of reaction-diffusion

Table 1. Parameter values.

Parameter	Symbol	Value	Source
Dimension of neutrophil layer	h_N or r_N	20–2000 μm	Diegelmann (2003); Fazli *et al.* (2011); Kragh *et al.* (2014)
Dimension of biofilm layer	h_B or r_B	5–1200 μm	Bjarnsholt *et al.* (2013)
Oxygen concentration at tissue interface	C_H	30–160 μM	Spence and Walker (1984)
Oxygen concentration at air interface	C_A	190–250 μM	*a*
First-order oxygen consumption rate for neutrophils	k_N	0.001–0.28 s^{-1}	*b*
First-order oxygen consumption rate for biofilm	k_B	0.017–1.7 s^{-1}	*c*
Diffusion coefficient of oxygen in neutrophil layer	D_N	1×10^{-5} cm^2 s^{-1}	Stewart (2003)
Diffusion coefficient of oxygen in biofilm layer	D_B	1×10^{-5} cm^2 s^{-1}	Stewart (2003)

[a] Air saturation at elevations from sea level to one mile.

[b] Rates from Bernstein, Humbert and Hliwa (1985), Green, Hill and Tew (1987) and Kolpen *et al.* (2010) normalized to 10^7 neutrophils per ml thenscaled up by a factor of 100 to apply to neutrophil densities of 10^9 neutrophils per ml (Fazli *et al.* 2011). This calculation result in zero-order rates of 25, 28 and 70 μM s^{-1}, respectively. Salva *et al.* (1996) suggests the possibility of even higher local neutrophil densities. Ordoñez *et al.* (2003) reported sputum neutrophil density of 8×10^6 cells per ml. First-order rate coefficients were determined by dividing the zero-order coefficients quoted above by the maximum concentration of oxygen in the system, 250 μM. This concentration corresponds to the dissolved oxygen concentration at equilibrium with air at sea level.

[c] Upper and lower values of biofilm zero-order oxygen consumption rate estimated from ($\mu X/Y_{xs}$)(mole/32 g)(10^6 μmole/mole)(h/3600 s) using ranges of possible specific growth rate (μ, 0.1 to 1 h^{-1}), yield coefficient (Y_{xs}, 0.5 to 1 g_X per gO_2) and cell density (X, 5 to 25 g_X per liter). This calculation results in zero-order rates that range from 4.3 to 434 μM s^{-1}. First-order rate coefficients were determined as explained in footnote *b* above.

Table 2. Parameter values for illustrative cases.

Case	(s^{-1}) k_B	(μm) h_B	(μm^2 s^{-1}) D_B, D_N	(s^{-1}) k_N	(μm) h_N	$\emptyset_B$	$\emptyset_N$	Scenario
A	0.01	10	1000	0.001	10	0.032	0.01	Both $\emptyset_B$, $\emptyset_N$ small
B	0.01	10	1000	0.1	1000	0.032	10	$\emptyset_N$ dominates
C	0.1	100	1000	0.01	100	1	0.32	Both $\emptyset_B$, $\emptyset_N$ intermediate
D	1	1000	1000	0.001	10	32	0.01	$\emptyset_B$ dominates
E	1	1000	1000	0.1	1000	32	10	Both $\emptyset_B$, $\emptyset_N$ large

These five cases correspond to the five panels of Figs 2, 4 and 6. The oxygen concentrations at the air and tissue boundaries have been taken as $C_A = 200$ μM and $C_H = 40$ μM, respectively.

modeling in the biofilm field (van Loosdrecht *et al.* 2002) as well as on computational models of host cell–microbe interactions (Oremland *et al.* 2016). In this article, we report analyses of reaction-diffusion problems in which biofilm and neutrophil regions adjoin each other without intermixing or overlapping. The models derived herein are geometrically simple and afford analytic solutions. Such models are clearly simplifications of reality. They do not incorporate multidimensional structures, mixed species interactions or external flows, all features that are known to occur in some biofilm systems and aspects that have been addressed in pioneering biofilm modeling work (Picioreanu, van Loosdrecht and Heijnen 1998; Cogan and Wolgemuth 2005; Alpkvist and Klapper 2007; Eberl and Sudarsan 2008). Here we extend classic biofilm reaction-diffusion models to include host interactions in the form of an adjoining neutrophil layer. To the best of our knowledge, this article is the first example of a reaction-diffusion analysis of a hybrid biofilm-neutrophil system. The value of analytical models as a starting point is that they can define overall behaviors of the system and point to likely biological relevance without introducing extra complexity.

MATERIALS AND METHODS

We analyze theoretically three simple geometries that may approximate the distribution of biofilm (Bjarnsholt *et al.* 2013; Stewart 2014) and neutrophils *in vivo* (Fig. 1). A classic model of biofilm structure is the flat slab. Here we allow for an adjoining layer containing neutrophils to create a two-layered slab structure (Fig. 1A). Such a disjoint layered structure is suggested by some microscopic observations (Diegelmann 2003; Zhao *et al.* 2010; Kragh *et al.* 2014). For a mucosal or dermal biofilm, one boundary of the biofilm will be an air interface and the other will be in tissue. Thus, we imposed specified oxygen concentrations along these boundaries. An implanted medical device constitutes a special case of the two-layered slab. In this case the biofilm is assumed to form a layer on the implant surface and is covered by a neutrophil-containing layer (Fig. 1B). The implant is assumed to be impermeable to oxygen so that a no-flux condition is imposed at this boundary. Recent discussions of the structure of infectious biofilms suggest that biofilms are often found as relatively small aggregates of microbial cells intermixed or covered with extensive host-derived material (Bjarnsholt *et al.* 2013; Stewart 2014). To capture this structure, concentric spheres of biofilm (at the core) and neutrophils (in a shell) are considered (Fig. 1C). Simplified geometric models can often capture the overall behavior of complex systems (Aristotelous *et al.* 2015).

First-order reaction kinetics of oxygen have been assumed for the consumption of oxygen by both bacteria and neutrophils. This is partly done for mathematical convenience as it permits exact analytical solutions. First-order kinetics provide a bound on the behavior expected from a more realistic saturation kinetic models such as Monod kinetics. The first-order approximation of saturation kinetics leads to the maximum extent of oxygen penetration. Thus, we anticipate that the actual occurrence of hypoxia will be more common and more severe than the current analysis predicts. Our results can be viewed as a conservative estimation of the importance of hypoxia in biofilm–host interactions.

Consider the steady-state reaction-diffusion equations in a two-layered slab (geometries in Fig. 1A and B),

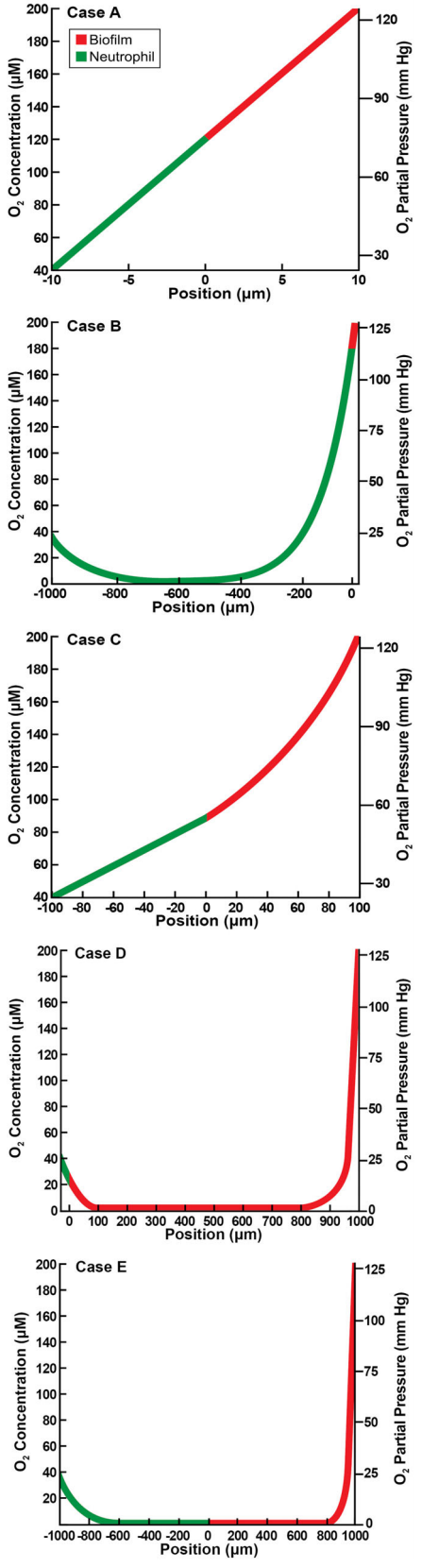

Figure 2. Oxygen concentration profiles in slab geometry bounded by air and host tissue for five illustrative cases as detailed in Table 2. Panels A–E correspond to the lettered cases in the table. Position is the value of spatial variable z, with $z > 0$ corresponding to the biofilm layer and $z < 0$ to the neutrophil layer.

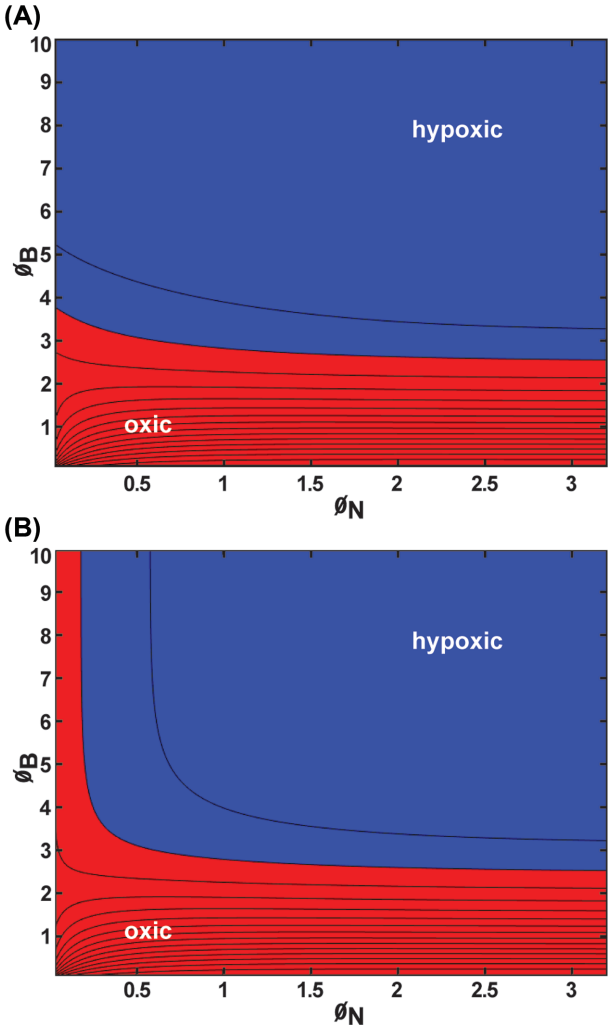

Figure 3. Oxygen concentration within the biofilm layer for slab geometry bounded by air and host tissue with first-order reaction kinetics presented as a contour plot: (A) minimum concentration within the biofilm; (B) concentration at the biofilm–neutrophil interface. Blue denotes values corresponding to hypoxia (less than 10 mm Hg oxygen); red denotes values that are oxic (greater than or equal to 10 mm Hg oxygen). Parameter values: $C_A = 200\ \mu M = 127.6$ mm Hg, $C_H = 40\ \mu M = 25.5$ mm Hg, $k_N = 0.01\ s^{-1}$, $k_B = 0.1\ s^{-1}$, $D_N = 1000\ \mu m^2\ s^{-1}$, $D_B = 1000\ \mu m^2\ s^{-1}$, h_N ranging from 10 to 1000 μm, h_B ranging from 10 to 1000 μm.

$$D_B \frac{d^2 C_B}{dz^2} - k_B C_B = 0 \quad (1)$$

$$D_N \frac{d^2 C_N}{dz^2} - k_N C_N = 0 \quad (2)$$

with interface conditions

$$C_B(0) = C_N(0) \quad (3)$$

$$D_B \frac{dC_B}{dz}(0) = D_N \frac{dC_N}{dz}(0). \quad (4)$$

The interface conditions stipulate continuity of oxygen concentration (Equation 3) and matching flux (Equation 4).

For the slab bounded by air and tissue (Fig. 1A), the boundary conditions impose fixed concentrations

$$C_B(h_B) = C_A;\ C_N(-h_N) = C_H\ . \quad (5)$$

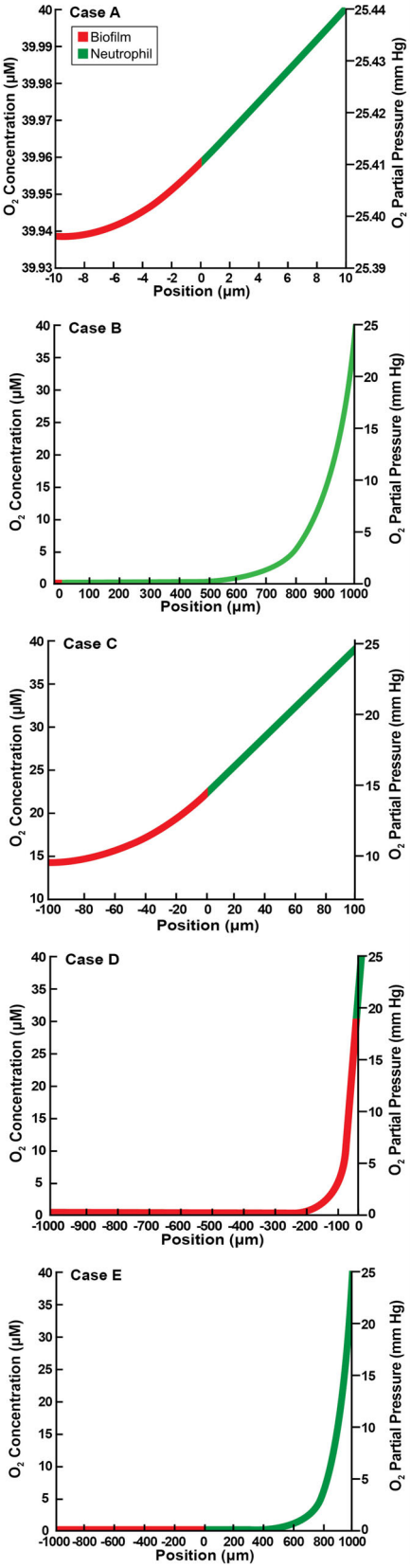

Figure 4. Oxygen concentration profiles in slab geometry bounded by an implant and host tissue for five illustrative cases as detailed in Table 2. Panels **A–E** correspond to the lettered cases in the table. Position is the value of spatial variable z, with $z < 0$ corresponding to the biofilm layer and $z > 0$ to the neutrophil layer.

The solutions are

$$C_N = \frac{\cosh\left(\emptyset_N \frac{z}{h_N}\right)}{\cosh \emptyset_N}\left[\frac{C_H \alpha \tanh \emptyset_B + C_A \frac{\sinh \emptyset_N}{\cosh \emptyset_B}}{\alpha \tanh \emptyset_B + \tanh \emptyset_N}\right] + \frac{\sinh\left(\emptyset_N \frac{z}{h_N}\right)}{\sinh \emptyset_N}\left[\frac{C_A \frac{\sinh \emptyset_N}{\cosh \emptyset_B} - C_H \tanh \emptyset_N}{\alpha \tanh \emptyset_B + \tanh \emptyset_N}\right] \quad (6)$$

$$C_B = \frac{\cosh\left(\emptyset_B \frac{z}{h_B}\right)}{\cosh \emptyset_B}\left[\frac{C_H \alpha \frac{\sinh \emptyset_B}{\cosh \emptyset_N} + C_A \tanh \emptyset_N}{\alpha \tanh \emptyset_B + \tanh \emptyset_N}\right] + \frac{\sinh\left(\emptyset_B \frac{z}{h_B}\right)}{\sinh \emptyset_B}\left[\frac{C_A \alpha \tanh \emptyset_B - C_H \alpha \frac{\sinh \emptyset_B}{\cosh \emptyset_N}}{\alpha \tanh \emptyset_B + \tanh \emptyset_N}\right] \quad (7)$$

where

$$\alpha = \left(\frac{k_N D_N}{k_B D_B}\right)^{1/2}; \quad \emptyset_B = \left(\frac{k_B h_B^2}{D_B}\right)^{1/2}; \quad \emptyset_N = \left(\frac{k_N h_N^2}{D_N}\right)^{1/2}. \quad (8)$$

The parameters $\emptyset_B$ and $\emptyset_N$ are dimensionless ratios of the reaction and diffusion rates known as Thiele moduli.

For the slab structure on the surface of a medical device (Fig. 1B), a no flux condition is required at the implant surface, which is assumed to be oxygen impermeable, and a fixed concentration is imposed at the interface with tissue

$$\frac{dC_B}{dz}(-h_B) = 0 \quad (9)$$

$$C_N(h_N) = C_H \quad (10)$$

In this case, the solutions are

$$C_B = C_H\, \alpha \frac{\cosh\left(\emptyset_B \frac{z}{h_B}\right) + \tanh \emptyset_B \sinh\left(\emptyset_B \frac{z}{h_B}\right)}{\tanh \emptyset_B \sinh \emptyset_N + \alpha \cosh \emptyset_N} \quad (11)$$

$$C_N = C_H \frac{\alpha \cosh\left(\emptyset_N \frac{z}{h_N}\right) + \tanh \emptyset_B \sinh\left(\emptyset_N \frac{z}{h_N}\right)}{\tanh \emptyset_B \sinh \emptyset_N + \alpha \cosh \emptyset_N} \quad (12)$$

Finally, we consider the scenario of a spherical core of microbial biofilm surrounded by a concentric shell of neutrophils (Fig. 1C). The steady-state reaction-diffusion equations in spherical coordinates are

$$\frac{1}{r^2}\frac{d}{dr}\left(r^2 D_B \frac{dC_B}{dr}\right) - k_B C_B = 0 \quad (13)$$

$$\frac{1}{r^2}\frac{d}{dr}\left(r^2 D_N \frac{dC_N}{dr}\right) - k_N C_N = 0 \quad (14)$$

with interface conditions

$$C_B(r_B) = C_N(r_B) \quad (15)$$

$$D_B \frac{dC_B}{dr}(r_B) = D_N \frac{dC_N}{dr}(r_B). \quad (16)$$

and boundary conditions

$$C_N(r_B + r_N) = C_H \quad (17)$$

$$r^2 \frac{dC_B}{dr}(0) = 0. \quad (18)$$

The solutions are

$$C_B = \frac{B_1 R}{r} \sinh\left(\emptyset_B \frac{r}{r_B}\right) \quad (19)$$

$$C_N = \frac{A_2 R}{r} \cosh\left(\emptyset_N\left(\frac{r-R}{r_N}\right)\right) + \frac{B_2 R}{r} \sinh\left(\emptyset_N\left(\frac{r-R}{r_N}\right)\right) \quad (20)$$

where

$$R = r_B + r_N;\ \ \emptyset_B = \left(\frac{k_B r_B^2}{D_B}\right)^{1/2};\ \ \emptyset_N = \left(\frac{k_N r_N^2}{D_N}\right)^{1/2} \quad (21)$$

$$B_1 = \frac{\alpha C_H}{\sinh\emptyset_N \sinh\emptyset_B \left(\frac{\alpha}{\emptyset_N}\frac{r_N}{r_B} - \frac{1}{\emptyset_B}\right) + \sinh\emptyset_N \cosh\emptyset_B + \alpha\cosh\emptyset_N \sinh\emptyset_B} \quad (22)$$

$$A_2 = C_H \quad (23)$$

$$B_2 = C_H \frac{\alpha\sinh\emptyset_N \sinh\emptyset_B + \cosh\emptyset_N \cosh\emptyset_B + \cosh\emptyset_N \sinh\emptyset_B \left(\frac{\alpha}{\emptyset_N}\frac{r_N}{r_B} - \frac{1}{\emptyset_B}\right)}{\sinh\emptyset_N \sinh\emptyset_B \left(\frac{\alpha}{\emptyset_N}\frac{r_N}{r_B} - \frac{1}{\emptyset_B}\right) + \sinh\emptyset_N \cosh\emptyset_B + \alpha\cosh\emptyset_N \sinh\emptyset_B} \quad (24)$$

Ranges of parameter values were drawn from the literature as summarized in Table 1 and five specific cases representing a spectrum of possibilities were analyzed (Table 2).

RESULTS

We calculated the spatial distribution of oxygen in systems consisting of adjoining layers of microbial biofilm and host neutrophils. Because both microorganisms and activated neutrophils consume oxygen, their concerted reactivity determines the local availability of oxygen. Of particular interest is the concentration of oxygen at the interface between the biofilm and neutrophil layers. The availability of oxygen at this juncture is likely important for the ability of neutrophils to exhibit microbiocidal activity and is the relevant concentration for this aspect since this is where the neutrophils contact microorganisms. We also examine the lowest concentration of oxygen within the biofilm layer, a minimum that is expected to be important in determining a shift from aerobic to anaerobic respiration or fermentative metabolism in the microbial community.

The solutions examined here are presented in terms of Thiele moduli, dimensionless numbers that compare the rates of reaction (of oxygen) and diffusion (also of oxygen). There are two Thiele moduli: one for the biofilm region ($\emptyset_B$) and another for the neutrophil region ($\emptyset_N$). When a Thiele modulus is small ($\emptyset$ $<$ 1), diffusive transport is fast compared to reaction. Conversely, when a Thiele modulus is large ($\emptyset$ $>$ 1), diffusive transport is slow compared to reaction and steep concentration gradients can develop.

We examine first the flat slab geometry that is bounded by air along one edge and host tissue on the other. These results correspond to the geometry diagrammed in Fig. 1A. The illustrative cases presented in Fig. 2 suggest a range of possible outcomes. Concentration minima are predicted in three of the five cases. Hypoxia at the biofilm–neutrophil interface is predicted in only one case (Fig. 2E), and hypoxia internally within the biofilm layer is predicted in two instances (Fig. 2D and E). (For convenience in this analysis, we define hypoxia as less than 10 mm Hg of oxygen.) When the Thiele moduli are relatively small, approximately linear concentration profiles are predicted (Fig. 2A and C). When one or both Thiele moduli is large, concentration minima and large hypoxic zones are predicted (Fig. 2B, D and E). The dimension of the region of hypoxia in these latter three cases ranges from approximately 0.5 to 1.7 mm.

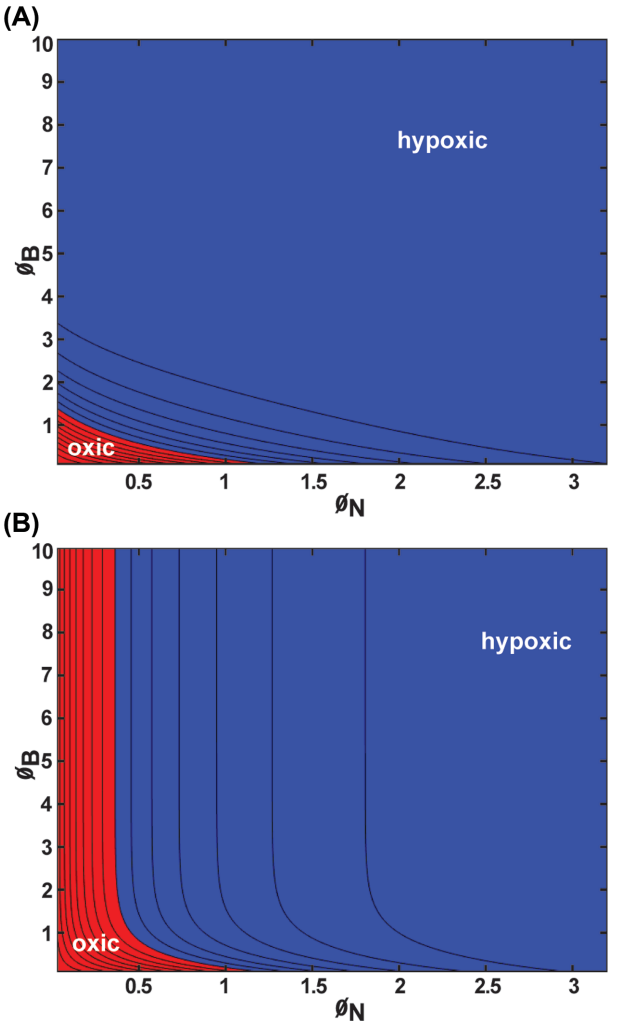

Figure 5. Oxygen concentration within the biofilm layer for slab geometry bounded by an implant and host tissue presented as a contour plot: (**A**) minimum concentration within the biofilm; (**B**) concentration at the biofilm–neutrophil interface. Blue denotes values corresponding to hypoxia (less than 10 mm Hg oxygen); red denotes values that are oxic (greater than or equal to 10 mm Hg oxygen). Parameter values: $C_A = 200\ \mu M = 127.6$ mm Hg, $C_H = 40\ \mu M = 25.5$ mm Hg, $k_N = 0.01\ s^{-1}$, $k_B = 0.1\ s^{-1}$, $D_N = 1000\ \mu m^2\ s^{-1}$, $D_B = 1000\ \mu m^2\ s^{-1}$, h_N ranging from 10 to 1000 μm, h_B ranging from 10 to 1000 μm.

To explore these outcomes further, the occurrence of hypoxia was plotted as a function of the two Thiele moduli (Fig. 3). Hypoxia develops within the biofilm (Fig. 3A) when the biofilm-associated Thiele modulus,$\emptyset_B$, is greater than about 3. Hypoxia develops at the biofilm–neutrophil interface if $\emptyset_B > 3$ and $\emptyset_N > 0.2$ (Fig. 3B).

Next, we consider the flat slab geometry that is bounded by an implant surface along one edge and host tissue on the other. These results correspond to the geometry diagrammed in Fig. 1B. The concentration of oxygen decreases monotonically from the host interface to a minimum at the implant surface in all of the illustrative cases presented in Fig. 4. Hypoxia at the biofilm–neutrophil interface is predicted in two cases (Fig. 4B and E), and hypoxia internally within the biofilm layer is predicted in four instances (Fig. 4A, B, D and E). To explore these outcomes further, the occurrence of hypoxia was plotted as a function of the two Thiele moduli (Fig. 5). Hypoxia develops within the biofilm when either $\emptyset_N$ or $\emptyset_B$ exceeds about

1 (Fig. 5A). Hypoxia develops at the biofilm–neutrophil interface if $\emptyset_N$ is larger than about 0.4 (Fig. 5B).

Representative oxygen concentration profiles for the concentric spherical structure (a biofilm core surrounded by a neutrophil shell) are plotted in Fig. 6. These results correspond to the geometry diagrammed in Fig. 1C. The profiles decrease monotonically to a minimum at the center of the structure; the lowest oxygen concentration experienced by the microorganisms occurs at this point. Hypoxia at the biofilm–neutrophil interface is predicted in two cases (Fig. 6B and E) and hypoxia within the biofilm in three cases (Fig. 6B, D and E). Hypoxia at the center is manifested when $\emptyset_B > 4$ or at smaller values of $\emptyset_B$ if $\emptyset_N$ is sufficiently large (Fig. 7A). In the spherical geometry, hypoxia at the biofilm–neutrophil interface requires that $\emptyset_N$ is greater than approximately 2 (Fig. 7B).

DISCUSSION

Locally reduced oxygen tension is a common feature of the *in vivo* biofilm. We analyzed the reaction-diffusion interactions that underpin the establishment of oxygen concentration gradients *in vivo*. The results support the conjecture that oxygen consumption by both microorganisms in the biofilm and host neutrophils can contribute to the development of hypoxic conditions in the vicinity of a biofilm infection. In all three geometries considered (biofilm near an air interface as in a dermal wound or mucus layer, biofilm on an implanted medical device, biofilm aggregates dispersed in mucus or tissue), hypoxia was predicted with a subset of plausible parameter values representing ranges of the oxygen consumption kinetics of microorganisms and neutrophils, oxygen diffusion coefficients, and biofilm and neutrophil region dimensions. Specifically, realistic conditions were found for all three scenarios analyzed that could lead to hypoxia at the biofilm–neutrophil interface or hypoxia in the interior of the biofilm layer.

These calculations suggest that hypoxia may manifest more readily on an implant (Fig. 5) than in a wound or lung mucosal biofilm (Fig. 3). The reasons for this are simply that the biofilm on the implant is supplied with oxygen at a lower concentration (in our analysis, 40 μM in the tissue rather than 200 μM at the gas interface) and the implant is supplied with oxygen from a single boundary rather than from both sides.

The oxygen concentration gradients we have calculated resemble those measured experimentally *in vivo* and *ex vivo* (Worlitzsch *et al.* 2002; Jesaitis *et al.* 2003; Kolpen *et al.* 2014; Cowley *et al.* 2015; James *et al.* 2016). Depletion of oxygen to hypoxic levels (here taken as below 10 mm Hg or 16 μM oxygen) was reported in five of the six measurements summarized in Table 3. The distance over which oxygen concentrations decreased from a maximum to minimum values ranged from 480 to 8850 microns. These distances are similar to those used in our calculations (Table 2). Oxygen gradients measured in mice with biofilm-infected wound scabs immediately after euthanization by James *et al.* 2016 found minima in oxygen concentration profiles that resemble those predicted here (Fig. 2D and E).

The finding that oxygen concentration at the interface of the biofilm and neutrophil layers can be diminished to hypoxic levels is biologically relevant because oxygen depletion will reduce neutrophil killing ability (Mandell 1974; Klebanoff 1980; Goldberg *et al.* 1995; Jesaitis *et al.* 2003). Neutrophil-mediated killing is dependent in part on the generation of reactive oxygen species from molecular oxygen. If the environment around a biofilm contains little oxygen, neutrophils will be impaired in their

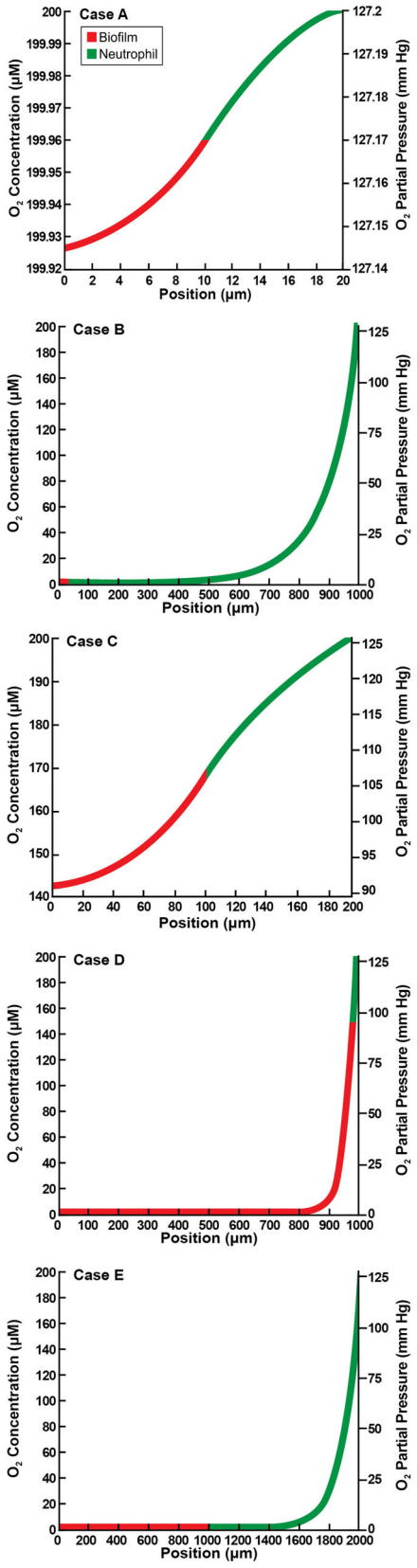

Figure 6. Oxygen concentration profiles in spherical geometry for five illustrative cases as detailed in Table 2. Panels **A–E** correspond to the lettered cases in the table. Position is the value of spatial variable *r*.

Table 3. Experimental measurements of oxygen concentrations in biofilm infection models.

Specimen	System	(μM) C_{max}	(μM) C_{min}	(μm) Δz	Source
Human neutrophils deposited on *P. aeruginosa* biofilm	*in vitro*	200	0	750	Jesaitis *et al.* (2003, fig. 5E)
Human CF sputum	*ex vivo*	150	0	8850	Kolpen *et al.* (2010, fig. 1B)
Human CF sputum	*ex vivo*	180–290	0	900–3800	Cowley *et al.* (2015, fig. 2C)
Cultured human wound debridement	*ex vivo*	219–227	3–6	700–1400	James *et al.* (2016, fig. 4)
Murine wound infection	*in vivo*	250	27–55	480–700	James *et al.* (2016, fig. 2A)
Human CF bronchial mucus	*in vivo*	280	4	NM	Worlitzsch *et al.* (2002, fig 2A and B)

NM—not measured.

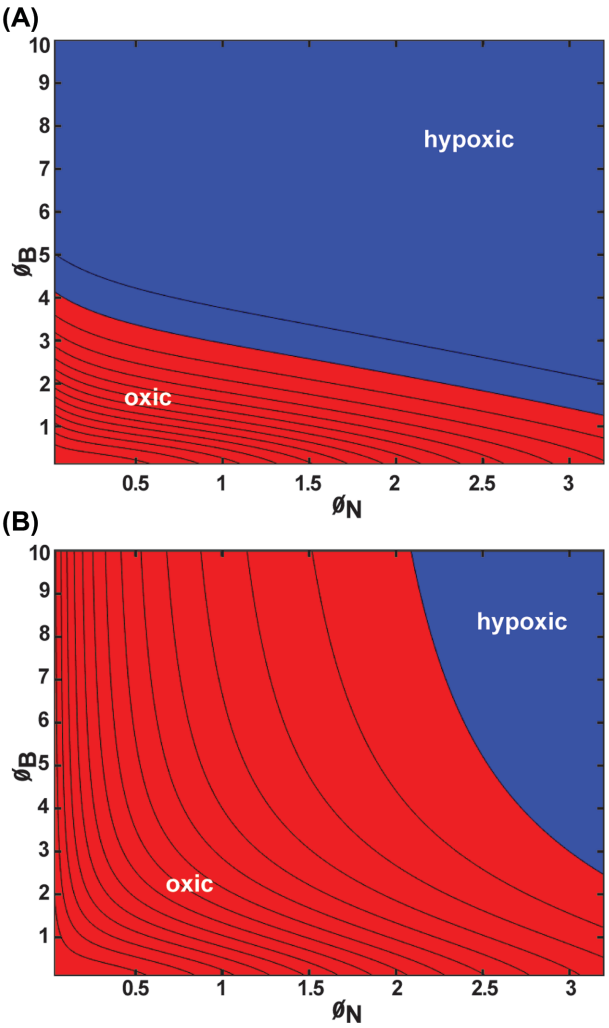

Figure 7. Oxygen concentration within the biofilm for spherical geometry presented as a contour plot: (**A**) minimum concentration within the biofilm; (**B**) concentration at the biofilm–neutrophil interface. In this geometry, the minima are always at the center of the composite structure. Blue denotes values corresponding to hypoxia (less than 10 mm Hg oxygen); red denotes values that are oxic (greater than or equal to 10 mm Hg oxygen). Parameter values: $C_A = 200$ μM = 127.6 mm Hg, $k_N = 0.01$ s^{-1}, $k_B = 0.1$ s^{-1}, $D_N = 1000$ μm^2 s^{-1}, $D_B = 1000$ μm^2 s^{-1}, h_N ranging from 10 to 1000 μm, h_B ranging from 10 to 1000 μm.

ability to generate reactive oxygen species such as hydrogen peroxide and hypochlorous acid. This impairment will compromise neutrophil ability to control and eliminate microorganisms.

The finding that hypoxia can readily establish within the biofilm layer is biologically relevant because this change in environment will likely alter microbial growth and metabolism. For a facultative anaerobic bacterium such as *P. aeruginosa*, oxygen depletion may limit microbial growth. Bacteria that enter an altered metabolic state in which the organism is less susceptible to antibiotics (Borriello *et al.* 2004; Field *et al.* 2005; King *et al.* 2010; Schaible, Taylor and Schaffer 2012; Gupta, Laskar and Kadouri 2016). For a facultative microorganism such as *Staphylococcus aureus*, oxygen limitation will likely cause a shift to a fermentative metabolism (Xu *et al.* 2016). With this shift, the bacterium acquires an advantage as it can sustain metabolic activity and continue to replicate whereas the host faces conditions that are not permissive of healing.

FUNDING

This work was supported by the National Institutes of Health General Medical Sciences [R01 GM109452 to PSS] and the National Science Foundation [1517100 to IK].

Conflict of interest. None declared.

REFERENCES

Alpkvist E, Klapper I. A multidimensional multispecies continuum model for heterogeneous biofilm development. *Bull Math Biol* 2007;**69**:765–89.

Alvarez-Ortega C, Harwood CS. Responses of *Pseudomonas aeruginosa* to low oxygen indicate that growth in the cystic fibrosis lung is by aerobic respiration. *Mol Microbiol* 2007;**65**:153–65.

Aristotelous AC, Klapper I, Grabovsky Y *et al.* Diffusive transport through a model host-biofilm system. *Phys Rev E* 2015;**92**:022703.

Bernstein JM, Humbert JR, Hliwa MM. Oxygen consumption of middle ear and peripheral blood neutrophils in acute suppurative otitis media. *Am J Otolaryngol* 1985;**6**:169–72.

Bjarnsholt T, Alhede M, Alhede M *et al.* The in vivo biofilm. *Trends Microbiol* 2013;**21**:466–74.

Bjarnsholt T, Kirketerp-Moller K, Jensen PØ *et al.* Why chronic wounds will not heal: a novel hypothesis. *Wound Repair Regen* 2008;**16**:2–10.

Borriello G, Werner E, Roe F *et al.* Oxygen limitation contributes to antibiotic tolerance of *Pseudomonas aeruginosa* in biofilms. *Antimicrob Agents Ch* 2004;**48**:2659–64.

Campbell EL, Bruyninckx WJ, Kelly CJ *et al.* Transmigrating neutrophils shape the mucosal microenvironment through localized oxygen depletion to influence resolution of inflammation. *Immunity* 2014;**40**:66–77.

Cogan NG, Wolgemuth CW. Pattern formation by bacteria-driven flow. *Biophys J* 2005;**88**:2525–9.

Costerton JW. Anaerobic biofilm infections in cystic fibrosis. *Mol Cell* 2002;**10**:699–700.

Costerton JW, Stewart PS, Greenberg EP. Bacterial biofilms: a common cause of persistent infections. *Science* 1999;**284**:1318–22.

Cowley ES, Kopf SH, LaRiviere A *et al.* Pediatric cystic fibrosis sputum can be chemically dynamic, anoxic, and extremely reduced due to hydrogen sulfide formation. *mBio* 2015;**6**:e00767.

Diegelmann RF. Excessive neutrophils characterize chronic pressure ulcers. *Wound Repair Regen* 2003;**11**:490–5.

Donlan RM, Costerton JW. Biofilms: survival mechanisms of clinically relevant microorganisms. *Clin Microbiol Rev* 2002;**15**:167–93.

Dowd SE, Sun Y, Secor PR *et al.* Survey of bacterial diversity in chronic wounds using pyrosequencing, DGGE, and full ribosome shotgun sequencing. *BMC Microbiol* 2008;**8**:43.

Downey DG, Bell SC, Elborn JS. Neutrophils in cystic fibrosis. *Thorax* 2009;**64**:81–88.

Eberl HJ, Sudarsan R. Exposure of biofilms to slow flow fields: the convective contribution to growth and disinfection. *J Theor Biol* 2008;**253**:788–807.

Fazli M, Bjarnsholt T, Kirketerp-Møller K *et al.* Quantitative analysis of the cellular inflammatory response against biofilm bacteria in chronic wounds. *Wound Repair Regen* 2011;**19**:387–91.

Field TR, White A, Elborn JS *et al.* Effect of oxygen limitation on the in vitro antimicrobial susceptibility of clinical isolates of *Pseudomonas aeruginosa* grown planktonically and as biofilms. *Eur J Clin Microbiol* 2005;**24**:677–87.

Frank DN, Wysocki A, Specht-Glick DD *et al.* Microbial diversity in chronic open wounds. *Wound Repair Regen* 2009;**17**:163–72.

Frankel YM, Melendez JH, Wang NY *et al.* Defining wound microbial flora: molecular microbiology opening new horizons. *Arch Dermatol* 2009;**145**:1193–5.

Goldberg JJ, Pankey JW, Politis I *et al.* Effect of oxygen tension on killing of Escherichia coli by bovine polymorphonuclear neutrophil leucocytes in vitro. *J Dairy Res* 1995;**62**:331–8.

Green MJ, Hill HA, Tew DG. The rate of oxygen consumption and superoxide anion formation by stimulated human neutrophils The effect of particle concentration and size. *FEBS Lett* 1987;**216**:31–34.

Gristina AG, Shibata Y, Giridhar G *et al.* The glycocalyx, biofilm, microbes, and resistant infection. *Semin Arthroplasty* 1994;**5**:160–70.

Gupta S, Laskar N, Kadouri DE. Evaluating the effect of oxygen concentrations on antibiotic sensitivity, growth, and biofilm formation of human pathogens. *Microbiol Insights* 2016;**9**:37–46.

Guss AM, Roeselers G, Newton IL *et al.* Phylogenetic and metabolic diversity of bacteria associated with cystic fibrosis. *ISME J* 2011;**5**:20–29.

Hall-Stoodley L, Costerton JW, Stoodley P. Bacterial biofilms: from the natural environment to infectious diseases. *Nat Rev Microbiol* 2004;**2**:95–108.

Han A, Zenilman JM, Melendez JH *et al.* The importance of a multifaceted approach to characterizing the microbial flora of chronic wounds. *Wound Repair Regen* 2011;**19**:532–41.

Hassett DJ, Sutton MD, Schurr MJ *et al.* Pseudomonas aeruginosa hypoxic or anaerobic biofilm infections within cystic fibrosis airways. *Trends Microbiol* 2009;**17**:130–8.

Hyde JA, Darouiche RO, Costerton JW. Strategies for prophylaxis against prosthetic valve endocarditis: a review article. *J Heart Valve Dis* 1998;**7**:313–5.

James GA, Ge Zhao A, Usui M *et al.* Microsensor and transcriptomic signatures of oxygen depletion in biofilms associated with chronic wounds. *Wound Rep and Reg* 2016;**24**:373–83.

James GA, Swogger E, Wolcott R *et al.* Biofilms in chronic wounds. *Wound Repair Regen* 2008;**16**:37–44.

Jensen ET, Kharazmi A, Lam K *et al.* Human polymorphonuclear leukocyte response to *Pseudomonas aeruginosa* grown in biofilms. *Infect Immun* 1990;**58**:2383–5.

Jesaitis AJ, Franklin MJ, Berglund D *et al.* Compromised host defense on *Pseudomonas aeruginosa* biofilms: characterization of neutrophil and biofilm interactions. *J Immunol* 2003;**171**:4329–39.

Kalani M, Ostergren J, Brismar K *et al.* Transcutaneous oxygen tension and toe blood pressure as predictors for outcome of diabetic foot ulcers. *Diabetes Care* 1999;**22**:147–51.

King P, Citron DM, Griffith DC *et al.* Effect of oxygen limitation on the in vitro activity of levofloxacin and other antibiotics administered by the aerosol route against *Pseudomonas aeruginosa* from cystic fibrosis patients. *Diagn Microbiol Infect Dis* 2010;**66**:181–6.

Klebanoff SJ. Oxygen metabolism and the toxic properties of phagocytes. *Ann Intern Med* 1980;**93**:480–9.

Kolpen M, Hansen CR, Bjarnsholt T *et al.* Polymorphonuclear leucocytes consume oxygen in sputum from chronic *Pseudomonas aeruginosa* pneumonia in cystic fibrosis. *Thorax* 2010;**65**:57–62.

Kolpen M, Kühl M, Bjarnsholt T *et al.* Nitrous oxide production in sputum from cystic fibrosis patients with chronic *Pseudomonas aeruginosa* lung infection. *PLoS One* 2014;**9**:e84353.

Kragh KN, Alhede M, Jensen PØ *et al.* Polymorphonuclear leukocytes restrict growth of *Pseudomonas aeruginosa* in the lungs of cystic fibrosis patients. *Infect Immun* 2014;**82**:4477–86.

Lyczak JB, Cannon CL, Pier GB. Lung infections associated with cystic fibrosis. *Clin Microbiol Rev* 2002;**15**:194–222.

Mandell GL. Bactericidal activity of aerobic and anaerobic polymorphonuclear neutrophils. *Infect Immun* 1974;**9**:337–41.

Morris NS, Stickler DJ, McLean RJ. The development of bacterial biofilms on indwelling urethral catheters. *World J Urol* 1999;**17**:345–50.

Ordoñez CL, Henig NR, Mayer-Hamblett N *et al.* Inflammatory and microbiologic markers in induced sputum after intravenous antibiotics in cystic fibrosis. *Am J Resp Crit Care* 2003;**168**:1471–5.

Oremland M, Michels KR, Bettina AM *et al.* A computational model of invasive aspergillosis in the lung and the role of iron. *BMC Syst Biol* 2016;**10**:34.

Passerini L, Lam K, Costerton JW *et al.* Biofilms on indwelling vascular catheters. *Crit Care Med* 1992;**20**:665–73.

Picioreanu C, van Loosdrecht MC, Heijnen JJ. Mathematical modeling of biofilm structure with a hybrid differential-discrete cellular automaton approach. *Biotechnol Bioeng* 1998;**58**:101–16.

Pihlstrom BL, Michalowicz BS, Johnson JN. Periodontal diseases. *Lancet North Am Ed* 2005;**366**:1809–20.

Price LB, Liu CM, Melendez JH *et al.* Community analysis of chronic wound bacteria using 16S rRNA gene-based pyrosequencing: impact of diabetes and antibiotics on chronic wound microbiota. *PLoS One* 2009;**4**:e6462.

Ruangsetakit C, Chinsakchai K, Mahawongkajit P *et al.* Transcutaneous oxygen tension: a useful predictor of ulcer healing in critical limb ischaemia. *J Wound Care* 2010;**19**:202–6.

Salva PS, Doyle NA, Graham L *et al.* TNF-alpha, IL-8, soluble ICAM-1, and neutrophils in sputum of cystic fibrosis patients. *Pediatr Pulmonol* 1996;**21**:11–19.

Schaible B, Taylor CT, Schaffer K. Hypoxia increases antibiotic resistance in *Pseudomonas aeruginosa* through altering the composition of multidrug efflux pumps. *Antimicrob Agents Ch* 2012;**56**:2114–8.

Schobert M, Jahn D. Anaerobic physiology of *Pseudomonas aeruginosa* in the cystic fibrosis lung. *Int J Med Microbiol* 2010;**300**:549–56.

Sen CK. Wound healing essentials: let there be oxygen. *Wound Repair Regen* 2009;**17**:1–18.

Sen CK, Roy S. Redox signals in wound healing. *Biochim Biophys Acta* 2008;**1780**:1348–61.

Sibley CD, Grinwis ME, Field TR *et al*. Culture enriched molecular profiling of the cystic fibrosis airway microbiome. *PLoS One* 2011;**6**:e22702.

Spence VA, Walker WF. Tissue oxygen tension in normal and ischaemic human skin. *Cardiovasc Res* 1984;**18**:140–4.

Stewart PS. Diffusion in biofilms. *J Bacteriol* 2003;**185**:1485–91.

Stewart PS. Biophysics of biofilm infection. *Pathog Disease* 2014;**70**:212–8.

Stewart PS, Zhang T, Xu R *et al*. Reaction–diffusion theory explains hypoxia and heterogeneous growth within microbial biofilms associated with chronic infections. *Biofilms Microbiomes* 2016;**2**:16012.

Taylor CT, Doherty G, Fallon PG *et al*. Hypoxia-dependent regulation of inflammatory pathways in immune cells. *J Clin Invest* 2016;**126**:3716–24.

Tunney MM, Field TR, Moriarty TF *et al*. Detection of anaerobic bacteria in high numbers in sputum from patients with cystic fibrosis. *Am J Respir Crit Care Med* 2008;**177**:995–1001.

van Loosdrecht MC, Heijnen JJ, Eberl H *et al*. Mathematical modelling of biofilm structures. *Anton Leeuw* 2002;**81**: 245–56.

Worlitzsch D, Tarran R, Ulrich M *et al*. Effects of reduced mucus oxygen concentration in airway *Pseudomonas* infections of cystic fibrosis patients. *J Clin Invest* 2002;**109**:317–25.

Xu Y, Maltesen RG, Larsen LH *et al*. In vivo gene expression in a *Staphylococcus aureus* prosthetic joint infection characterized by RNA sequencing and metabolomics: a pilot study. *BMC Microbiol* 2016;**16**:80.

Xu KD, Stewart PS, Xia F *et al*. Spatial physiological heterogeneity in *Pseudomonas aeruginosa* biofilm is determined by oxygen availability. *Appl Environ Microb* 1998;**64**:4035–9.

Yoon S, Hennigan RF, Hilliard GM *et al*. *Pseudomonas aeruginosa* anaerobic respiration in biofilms. *Dev Cell* 2002;**3**:593–603.

Zemanick ET, Sagel SD, Harris JK. The airway microbiome in cystic fibrosis and implications for treatment. *Curr Opin Pediatr* 2011;**23**:319–24.

Zhao G, Hochwalt PC, Usui ML *et al*. Delayed wound healing in diabetic (db/db) mice with *Pseudomonas aeruginosa* biofilm challenge: a model for the study of chronic wounds. *Wound Repair Regen* 2010;**18**:467–77.